

Thermal Conductivity, Heat Sources and Temperature Profiles of Li-ion Batteries

Odne S. Burheim^{*a,b}, M. A. Onsrud^c, J.G. Pharoah^{d,e}, F. Vullum-Bruer^c
and P.J.S. Vie^g

^aDep. of Electr. and Comp. Engin., HiST - Sør-Trøndelag University
College, Trondheim, Norway.

^bDep. Chem., NTNU - Norwegian Univ. of Sci. and Technol., Trondheim,
Norway

^dQueen's-RMC Fuel Cell Research Centre, Kingston, ON, Canada

^eMechanical and Materials Engineering, Queen's University, Kingston,
ON, Canada

^cDep. of Mat. Sci. and Engin., NTNU - Norwegian Univ. of Sci. and
Technol., Trondheim, Norway

^gIFE - Institute for Energy Research, Kjeller, Lillestrøm, Norway

Abstract

In this paper we report the thermal conductivity of several commercial and non-commercial Li-ion secondary battery electrode materials with and without electrolyte solvents. We also measure the Tafel potential, the ohmic resistance, reaction entropy and external temperature of a commercial pouch cell secondary Li-ion battery. Finally we combined all the experimentally obtained data in a thermal model and discuss the corresponding internal temperature effects.

The thermal conductivity of dry electrode material was found to range from 0.07 to 0.41 W K⁻¹ m⁻¹ while the electrode material soaked in electrolyte solvent ranged from 0.36 to 1.10 W K⁻¹ m⁻¹. For all the different materials it was found that adding the electrolyte solvent increased the thermal conductivity by at least a factor of three. For one of the anode materials it was found that heat treatment at 3000 K increased the thermal conductivity by a factor of almost five.

Measuring the electric heat sources of an air cooled commercial pouch cell battery at up to $\pm 2C$ and the thermal conductivity of the electrode components made it possible to estimate internal temperature profiles. Combining the heat sources with tabulated convective heat transfer coefficients of air allowed us to calculate the ambient temperature profiles. At 12C charging rate (corresponding to 5 minutes complete charging) the internal temperature differences was estimated to be in the range of 4-20K, depending on the electrode thermal conductivity. The external temperature drop in air flowing at the battery surface was estimated to nearly 40K. Evaluating thermal

*Corresponding author; odnesb@hist.no

management of batteries in the light of our measurement led to the conclusion that external cooling is more challenging than internal, though neither should be neglected.

Introduction

The Li-ion secondary battery is currently one of the most viable battery options for automotive applications when weight is considered. However, Li-ion secondary batteries do not alone hold the potential for personal automotive vehicles with driving range much longer than 100 miles (160 km) unless one takes voluminous or heavy vehicles into account [1]. Combining a moderately sized battery package with a small fuel cell as a hybrid solution offers an optimum trade off between weight, driving range, refuelling time and power dynamics [2]. Also when evaluating well to wheel efficiency for almost any regional scenario this hybrid comes out on top (the exception being hydrogen from fossil-electric-powered-electrolysis) [2]. In addition to offering the commodity in assisting efficient automotive applications, Li-ion secondary batteries are also reasonably easily recycled [3].

When increasing the size of secondary batteries, particularly during intense charging, thermal management of batteries becomes important. Whereas the thermal management of low temperature fuel cells, Li-ion optimum battery hybrid partner, is starting to become reasonably well understood with respect to operation [4], ageing [5] and cooling [6], component thermal conductivity and heat management of secondary Li-ion batteries are still not thoroughly investigated [7, 8]. The same can be said for supercapacitors, another electrochemical component that goes into a robust hybrid system, see [9] and references therein. In the literature, there are mainly two approaches regarding heat handling for Li-ion secondary batteries; 1) developing flame retardant and thermal sustainable components, e.g. [10–14] and 2) managing the heat generated by reversible processes, e.g. [15–17]. Studies considering temperature effects above 200°C are not included in this study.

Heat and Temperatures in Li-ion Secondary Batteries

The Li-ion secondary battery can potentially convert the chemical free energy stored in the battery into electric work with efficiencies of more than 85-90% [18–20]. Despite this high efficiency there is always energy dissipated as heat associated with electrochemical cells [21–24]:

i) Battery reaction entropic heat. The temperature multiplied by the change in the reaction entropy and the current divided by the Faraday constant, $T\Delta S_j/nF$, is a reversible and inevitable heat source in a Li-ion secondary battery and is, according to the second law of thermodynamics, the minimum discharge heat. For commercial cells, the battery total reaction entropy depends mainly on the cathode composition. This is because the anode material is more or less the same for all types of commercial batteries. Depending on electrode material combinations such as LiCoO₂-carbon, LiFePO₄-titanate and LiNi_{0.7}Co_{0.3}O₂-carbon the reaction entropy of discharge is $\sim 35, \sim 27$ and ~ 17 J mol⁻¹ K⁻¹, correspondingly, whereas it is between 5 to 15 J mol⁻¹ K⁻¹ for most other reported Li-ion secondary batteries [25].

ii) The Tafel (or Butler-Volmer) equation predicts that increased current densities (reaction

rates) necessarily result in a parasitic loss, i.e. a reduction in the cell potential by an over-potential, η . This is the origin of the second heat source which is numerically the product of the current and the over-potential, ηj [26]. For Li-ion secondary batteries this term is very small compared to e.g. the oxygen red/ox electrode reaction.

iii) The Ohmic heat which is due to the ohmic resistance, R_{Ω} , multiplied with the square current density $R_{\Omega}j^2$. Its contribution is predominant in the electrolyte/separator region of the battery and to some degree also the solid electrolyte interface, SEI. Later, when we report measurements including electrodes with electrolyte solvents - we mean electrolyte solvents only rather than the combination of electrolyte and electrolyte solvent. The electrolyte salts were omitted due to hazardous reaction with air.

The second *ii*) and the third term *iii*) represent irreversible processes (lost work) whereas the first term *i*) is dictated by the sign of the entropy change for the reversible reactions in the two electrodes. In the case of a Li-ion battery however, all three terms represent heat generation during discharge, whereas the first term represents a heat sink and the two last terms heat sources during charging. Fully charging a battery electric vehicle (BEV) in five minutes (considering less than 85% charging efficiency when 12C charging is applied) allowing it to drive up to 500 km (300 miles) would require a power of 0.5 MW [1]. In such cases, it might well be that large reversible heats ($T\Delta S$) become desirable as an internal heat sink for charging. In fact, engineering electrode materials by implementing second components that adsorb heat by phase change have been proposed. The phase change adsorbs heat during intense loads, thus acting as a buffer [15, 16]. The convenience of the latter form of buffered heating comes at the expense of increased weight and increased amounts of flammable material in case of fires.

Heat Conduction in Porous Media

In general, improving performance of most heterogeneous reactors, such as electrochemical accumulators, is equivalent to increasing the surface area per volume. This is obtained by deploying porous materials with reduced particle size. Secondary Li-ion batteries are no exception from this. Neither are supercapacitors and fuel cells. A part of the perspective and motivation for this paper is to compare secondary Li-ion battery electrodes heat management properties to those of other electrochemical energy storage systems. In aiming at high loads, knowledge of denominators is useful. Hence the following comparison.

Heat generation in Li-ion batteries necessarily results in internal and external temperature gradients. With the heat sources mainly being in or adjacent to the electrolyte/separator region, the thermal conductivity of the electrode materials sandwiching this region is a key property for internal thermal gradients. Moreover, modern prismatic pouch cells consists of stacks of these cells through which the heat is conducted. In the earliest thermal Li-ion battery models, the thermal conductivities deployed were assumed to be similar to those of the solid materials rather than the porous versions of them [27]. Porous materials have, however, much lower thermal conductivities than dense ones [9, 28].

The situation for the Li-ion battery is, as mentioned, that both the anode (carbon based) and the cathode (mixed metal oxides) have highly porous structures. Looking first at the anode, this material can be compared to that of electrodes in supercapacitors [9] or micro porous layers, MPL, used in the polymer electrolyte fuel cells, PEMFC, [29]. As already

Table 1: Various thermal conductivities reported, suggested and applied for Li-ion batteries in the literature.

Material	k W K⁻¹ m⁻¹	Reference
Anode: Porous graphite soaked with paraffin	13-15	[17]
LiCoO ₂ / Carbonaceous electrode	1.58 / 1.04	[30]
Battery Average	32.2	[31]
Pouch Battery Assembly under load	0.9-3.4	[32]
Pouch Cell Exp. and Model Compared	0.25	[33]
Dry Battery Electrode materials	0.07-0.41	This study
Electrodes soaked in electrolyte solvent	0.36-1.26	This study

mentioned, the thermal conductivity of PEMFC components is much more studied than that of Li-ion batteries. Thus, comparing the materials of these two electrochemical systems serves as a good starting point when studying thermal gradients and material thermal conductivity of Li-ion batteries.

In this section we discuss accepted and our presented knowledge of thermal conductivity for Li-ion secondary batteries, supercapacitors, and some PEMFC components. All these materials are porous and typically contain a liquid. Secondary Li-ion battery and supercapacitor electrode materials contain organic electrolyte solvents mixed with inorganic salts while the PEMFC to some degree contain water. Secondary Li-ion anodes consists of carbon and PVDF and cathode of small particle of mixed metal oxides that are sintered, agglomerated, fused, and often calendered particles. Supercapacitor electrodes consists of carbon particles (activated carbon, carbon nanotubes, onion-like carbon, or a combination) and polytetrafluorethylene, PTFE, binder that is calendered [9]. A MPL of a PEMFC consists of activated carbon mixed with PTFE that is not calendered [29]. Because, in this study, the electrodes investigated are not calendered, this comparison is required at this point. In the study by Burheim et al. where the thermal conductivity of the MPL was investigated, it was observed that when the MPL was compressed up to around 10 bar, the MPL became incompressible and obtained a thermal conductivity of approximately $0.10 \text{ W K}^{-1} \text{ m}^{-1}$, when completely dry [29]. In this study, it was also observed that a PTFE content varying between 10 and 25 wt% did not impact the value of the dry thermal conductivity. Comparing to another study of Burheim et al., calendered activated carbon containing 5 wt% PTFE had a thermal conductivity of $0.13 \text{ W K}^{-1} \text{ m}^{-1}$ and that this value was independent of compaction pressure [9]. It is shown by many that very low PTFE contents in porous carbon can lead to this difference in thermal conductivity [34–36]. Overall, this shows that measuring thermal conductivity of porous carbon structures of the type that we study here, can be done at around 10 bar compaction pressure and that for dry porous materials it will not matter for the thermal conductivity whether or not these materials are calendered.

An overview of various reported thermal conductivities for Li-ion secondary batteries is given in Table 1. One can see that within the literature, thermal conductivities in the range of $0.25\text{-}32 \text{ W K}^{-1} \text{ m}^{-1}$ are reported for Li-ion secondary batteries [17, 30–33]. Kim studied and modelled dynamic temperature rises from a Li-ion pouch cell battery by adding several

thermocouples on the surface, concluding the thermal conductivity was close to $0.25 \text{ W K}^{-1} \text{ m}^{-1}$ [33]. This is in agreement with results of this paper. Nagpure et al. reported the thermal diffusivity of an entire Li-ion battery pouch cell to be $2\text{-}4 \cdot 10^{-7} \text{ m}^2\text{s}^{-1}$ by using a laser flash technique [37]. (For reference, the thermal diffusivity and conductivity of water is $0.14 \cdot 10^{-7} \text{ m}^2\text{s}^{-1}$ and $0.58 \text{ W K}^{-1} \text{ m}^{-1}$, respectively. The thermal diffusivity is equal to the thermal conductivity divided by the heat capacity and the material density.) In the absence of the heat capacity and material density, it is impossible to assess the thermal conductivity from the thermal diffusivity. Also, since the battery as a whole most likely have anisotropic thermal conductivity, heat capacity and density (due to the lamellar layers) the laser flash approach is very difficult to deploy with the purpose of determining Li-ion battery components thermal conductivity. The approach reported in this paper is the best suited available for electrode thermal conductivity measurements and the only one that allows for modification of the battery electrode material by adding electrolyte solvents.

Thermal modelling of Li-ion battery

Several studies report to some extent thermal management by the means of modelling for Li-ion batteries, according to Sato [24]. Cylindrical batteries, for instance, are mainly examined with respect to internal [30, 38] *or* external [31] temperature gradients and thermal management. Bandhauer et al. recently reviewed more than a hundred papers with respect to thermal handling of Li-ion batteries [8], stating that studies including both internal and external temperature profiles in combination with measurements is almost absent and indeed needed for battery electric vehicle (BEV) and hybrid electric vehicle (HEV) battery development. In this paper we focus on measuring thermal conductivity of the electrodes and implement this thermal model that includes only internal temperature profiles. Another motivation for this study was also to study some of the commercial batteries that are tested and to get a first hand overview of what the internal temperature is during cycling. Although the model is a simplification of the real world (2D not 3D), it demonstrates the need for the measurements presented in this paper.

Procedures

Thermal Conductivity Measurements

Measurement Methods When measuring thermal conductivities, one can apply transient methods and stationary methods. Transient methods traditionally consist of measuring the temperature response of a material when exposed to some surface or body with a given temperature. This is modernized by flashing a laser beam onto one side of a flat sheet followed by reading the temperature response by the use of an infra-red camera on either side. As mentioned, this approach requires knowledge of the heat capacity and material density in order to obtain more than the thermal diffusivity data [39]. In the case of Li-ion batteries there has been some doubt about the feasibility of using this technique and obtaining realistic values for the thermal conductivity [8]. The second approach for measuring thermal conductivity is stationary and typically consists of sandwiching a material between

two cylinders containing a series of thermocouples measuring an overall temperature difference, described in detail later. This method was also chosen by Alrashdan et al. and is the most suitable for the Li-ion battery electrodes due to the *porous structure* and the *unknown heat capacity* [17].

One very important topic discussed within the literature of thermal conductivity measurements deploying the stationary approach, is the relation between thermal conductivity of the sample, the contact resistance between the sample and the apparatus and also the contact resistance between stacked samples [40]. (These contacts were not accounted for by Alrashdan et al. [17]). Ramousse et al. stated that the thermal contact resistance of a fibrous material should be bound by the resistance of layers of either air or carbon with the thickness of an individual PTL fibre. For our materials this is equivalent to a layer as thick as half the average particle size with a thermal conductivity ranging between air and graphite. The challenge with a finite contact resistance between individual layers in a stack is that for every added sample one also adds one more sample-sample contact thermal resistance and hence, due to this linear relation between equations and unknowns, one is stuck with a matrix with no determinant. When using materials with a metal layer and porous electrodes, this problem becomes more complex as the thickness is increased but not the thermal resistance. A discussion of these implications follows with the results.

Apparatus The apparatus used in the experiments is depicted in Fig. 1 and is described in greater detail in [36]. The thermal conductivity apparatus measures all the variables that appear in a discrete form of Fourier's law [41], i.e. the heat fluxes q_i , the sample thickness, δ_s and the temperature drop over the sample. The heat flux is measured in stainless steel (q_{steel}) cylinders on each side of the investigated samples along with the temperature drop over the sample ($T_4 - T_5$) and the thickness of the sample material stacks (δ_{sample}), as in Eq. 1-3. In this context the term "sample" refers to a pile of materials subject to investigation and also the contact region to the apparatus. The heat fluxes in the cylinders, $q_{upper/lower}$, deviated less than 2% from each other. This corresponds to the precision of measuring the temperature differences between each of the thermocouples.

Next, the thermal resistance and its contact to the apparatus were plotted as a function of the measured thickness in order to separate the different resistance contributions of the stack components in a similar way as before [36, 40]. This was subsequently used for determining the thermal conductivity and the thermal contact resistance in the experiment. The samples were always stacked under the assumption that the thermal contact between each layer could be neglected, an assumption that was verified in this study as well as in others [29, 36]. One of the anode materials was measured both by changing the thickness of the porous layer and by stacking samples with constant layer thickness in order to demonstrate the validity of this assumption. This is shown in the result section.

All the measurements were carried out at 9.3 bar compaction pressure in order to ensure reasonable and reproducible contact between the sample and the apparatus. (Lowering the compaction pressure is known to give higher scatter in the measurements, see e.g. [5].) Another important reason for the chosen compaction pressure is that we know that it is so large that at least porous carbon becomes incompressible, see the introduction for a more detailed discussion. The upper temperature was set to 35 °C while the lower temperature was maintained at 10 °C such that the average sample temperature is very close to room

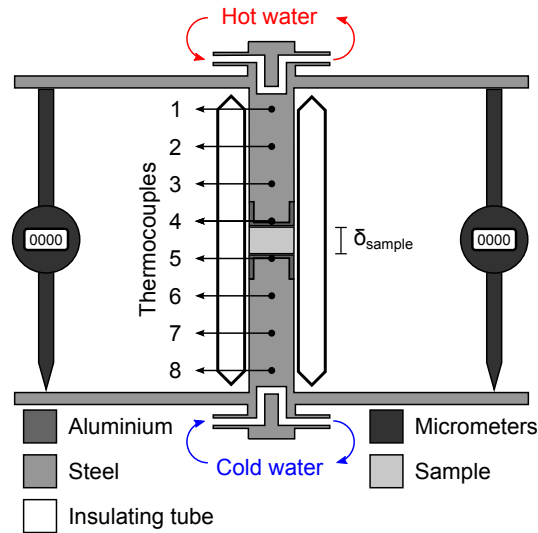


Figure 1: A 2D sketch of the apparatus used to measure thermal conductivity as reported here. [36].

temperature. The temperatures were fixed by circulating water from external reservoirs. q_i , k_i , T_i , δ_{i-j} and R_i are the heat flux, thermal conductivity, temperature, length/thickness and thermal resistivity of region, position or material in agreement with Fig. 1, respectively.

$$q_{upper} = k_{steel} \frac{T_1 - T_3}{\delta_{1-3}} \quad (1)$$

$$q_{lower} = k_{steel} \frac{T_6 - T_8}{\delta_{6-8}} \quad (2)$$

$$q_{sample} = \frac{q_{upper} + q_{lower}}{2}, \quad \text{and}; \quad R_{sample} = \frac{T_4 - T_5}{q_{sample}} \quad (3)$$

Material Selection The electrode materials selected for investigation were commercially available graphite based anodes (Timcal TIMREX[®] SLP 50) together with commercial LiCoO₂ cathode material from MTI Corporation. In addition, two classes of an in-house carbon material were tested, namely as-produced carbon cones (CCRAW) and carbon cones heat treated at 2700°C (CC2700). The carbon cone based material is a mixture of hollow cones and flat disks of carbon. The as-produced material consists of a crystalline core with a disordered outer shell [42], while CC2700 is graphitized, i.e. SEM and XRD shows that heat treatment makes the material more crystalline. The carbon cone material originally also contain some residual carbon black, though the content is not certain. All electrode materials are presented in Table 2. (The term D90 means that 90% of the particles are less than the given size.) The carbon was cast onto a copper film (12 μm thick) with a casting knife (K Control Coater from RK PrintCoat Instruments Ltd.) in the desired thickness whereas the LiCoO₂ material were precasted by the manufacturer onto a Al film (8 μm thick). The mixture consisted of 95 wt% of dry powder and 5 wt% binder polyvinylidene flouride (PVDF, Kynar 761), together with a solvent, 1-methyl-2-pyrrolidinone (NMP,

Table 2: Material selection for thermal conductivity and its properties.

Properties	LiCoO ₂	SLP50	CCRAW	CC2700
Type	comm. cathode	comm. anode	as-produced	annealed at 2700°C
Current coll.	aluminium foil	copper foil	copper foil	copper foil
Shape	potato	flat potato	cones / disks	cones / disks
Particle size	19 μ m (D90)	45 μ m (D90)	0.5 - 4 μ m	0.5 - 4 μ m
Structure	layered rock-salt	graphitic	dissord. carbon	graphitic
Capacity	145 mAh/g ^a	300 mAh/g ^b	195 mAh/g	305mAh/g ^b
Density	2.1 - 2.9 g/cm ³ ^c	0.49 g/cm ³ ^d	0.04 g/cm ³	0.07 g/cm ^{3d}
BET surface	–	6 m ² /g ^e	20	15 m ² /g ^f

^a For first discharge at 1C current rate, reported by manufacturer. ^b For the 100th cycle at C/4 current rate, tested in-house. ^c Tap Density, reported by manufacturer. ^d Bulk density, measured in-house. ^e Reported by manufacturer. ^f Measured in-house.

Sigma-Aldrich). The PVDF content was added until the material would be a dispersed smooth spread.

The materials were subject to measurements both for dry and electrolyte solvent soaked materials. A 50:50 wt% mixture of ethylene carbonate (Sigma-Aldrich) and diethyl carbonate (Aldrich) was used as electrolyte solvent. The salt was omitted due to toxicity and to avoid unwanted reactions with air. The electrolyte solvent was added to the electrode surfaces with a dropper before assembling pairs in the apparatus. In this way we assured residual solvent and fully wetting of the electrodes. The apparatus was subsequently sealed with a soft polymer film (Parafilm[®] M Barrier Film) and next insulated with expanded polyester. Unless the apparatus is sealed immediately, the electrolyte solvent will attract humidity from the air. The measurements were carried out during the winter and the relative humidity was therefore low.

Measurement Procedure Based on a reasoning from Ramousse et al. [40] combined with our own experience [36], two porous surfaces merging and two flat surfaces adjacent results in much lower contact region resistances compared to that of a flat and a porous surface in contact. Therefore, the electrodes when subject to thermal measurements were inserted in pairs in the apparatus. Each pair consisted of two discs of electrode materials on a metal substrate such that the electrode material of each disc would face the other and the metal substrate be at the outer surface. These would then either touch the apparatus or another paired sample. Because the carbon based electrodes were cast in-house, the thickness was controlled at three levels and only single pair of sample subject at the time in addition to stack samples of the same size. The LiCoO₂ sample however was used as one, two or three pairs at the time, respectively. Each sample was left for at least 15 minutes in order to reach a steady state temperature profile in the rig and then the temperature data was recorded at 30 second intervals for 10 minutes and averaged.

Deconvolution of Resistances in Series In order to deconvolute thermal resistances, one approach is to change the thickness of the sample, if possible. This can be seen by Eq. 4, where the only variable between the three experiments of the anode carbon material is the thickness (δ). This is despite that the contact resistances of the copper-apparatus

(App-Cu) and the two carbon anodes (C.A.-C.A.) can not be individually determined. The linearity between the sample resistance, as given by Eq. 3 and the thickness allows us to precisely determine the thermal conductivity of the carbon anode material ($k_{C.A.}$) from the slope without considering the offset thickness of the copper substrate film.

$$R_{sample} = 2R_{App-Cu} + R_{C.A.-C.A.} + \frac{\delta}{k_{C.A.}} \quad (4)$$

Regarding the series of the thermal resistances of the LiCoO_2 material on the Al substrate, the procedure is less straight forward and assumptions for simplifications are needed. Equation 5 gives the relation between all the thermal resistances for the experiment where pairs of LiCoO_2 on Al substrates are stacked in the apparatus. The first assumption is that the LiCoO_2 - LiCoO_2 and the Al-Al substrate film thermal contact resistances can be neglected. Metal-metal contacts are often not negligible because metals are relatively hard at the surface interaction, however in our case we have very pure and thin metal films, making this contact likely negligible since Al is soft and flat. The next assumption is that the thermal bulk resistance of the aluminium film can be neglected as the film thickness is $8 \mu\text{m}$ and the thermal conductivity of aluminium is $\sim 200 \text{ W K}^{-1}\text{m}^{-1}$. This is derived in Eq. 6. It follows from this that in obtaining the thermal conductivity, the sample resistance must be plotted as a function of the sample thickness minus the Al total film thickness, i.e. $\delta_{\text{LiCoO}_2} = \delta_{\text{sample}} - \delta_{\text{Al film}}$.

$$R_s = 2R_{App-Al} + (n_{\text{pair}} - 1)R_{Al-Al} + n_{\text{pair}}R_{\text{LiCoO}_2-\text{LiCoO}_2} + n_{\text{pair}}R_{\text{LiCoO}_2-\text{Layer}} + n_{\text{pair}}R_{Al-\text{film}} \quad (5)$$

$$R_s = 2R_{App-Al} + \frac{\delta_{\text{LiCoO}_2}}{k_{\text{LiCoO}_2}} + \left(\frac{\delta_{\text{Al film}}}{k_{\text{Al film}}} \right) \approx 2R_{App-Al} + \frac{\delta_{\text{LiCoO}_2}}{k_{\text{LiCoO}_2}} \quad (6)$$

Statistical Analysis and Accuracy of the Measurements The thermal conductivity apparatus was calibrated using materials with known thermal conductivities. These values are known with 5% accuracy and thus this level is the accuracy limitation of the reported values in this paper. However, the errors of the thermal conductivities reported in the results section deviate from the linear regression by the means of a least square of residual approach. This allows for the reported errors to appear more accurate. All data are reported with double standard deviations.

Commercial Li-ion Pouch Cell

Having access to relatively large scale batteries (range of 16-19 Ah) made for EV and HEV is valuable when estimating appropriate modelling conditions. One can measure the three most important heat source/sink parameters of the battery, i.e. the battery reaction entropy (*i*), Tafel heat (*ii*), and the ohmic resistance (*iii*). The Tafel overpotential and battery entropy measurement procedures are given in appendixes A and B.

Table 3: Entropy of electrode reactions, ΔS , [25] thermal conductivities, k_i , [17, 43], [present] and electric conductivities, $\sigma_{electrolyte}$, [44] used for the model of this study.

Entropy - ΔS	$/ \text{J mol}^{-1} \text{K}^{-1}$	Overpotential - η	$/ \text{mV}$
	9	-41.5	+66.5 log [j]
Material Layer	k_i $/ \text{W K}^{-1} \text{m}^{-1}$	κ S m^{-1}	δ_i $/ 10^{-6} \text{m}$
Carbon Anode	0.07-1.26	–	95
MixMeO	0.36-1.10	–	80
Electrolyte/Separator	0.2	0.0075	15

In order to keep the focus of this paper to the relation between heat generation, electrode material thermal conductivity and corresponding temperatures, the measurement using the pouch cells for obtaining the overpotential and the reversibel heat are placed in the appendixes, A and B.

Thermal Modelling

The presented model considers a repeated geometry of unit cells, with the same geometry as those in the investigated pouch cell. In the pouch cell, the unit cells are coupled in parallel. This is done such that anodes and cathodes pairwise share a current collector. In total, the battery contained 24 cells. In the present model we consider the unit cells to be repeated, as if they were coupled in series. Because this model only considers transport of heat by conduction, this is a simplification of no significance to the thermal effects. (The thermal resistances are coupled in series regardless of the order of the electrode configuration, i.e. anode-anode-cathode-cathode-... *versus* anode-cathode-anode-cathode-anode-....)

Physical Properties The electrical and physical properties needed for the model are given in Table 3. This includes for the reversible heat, the sources of irreversible heat; the electric conductivity and the kinetics (Tafel potentials - η), the thermal conductivities and the layer thicknesses. The nature of the heat sources were described in more detail the introduction and the way they are obtained is shown in Appendix A and B. The thicknesses stem from disassembling various commercial batteries in our laboratory. Figure 2 summarizes the geometry assembly. In addition, we consider the battery to be wrapped in an insulating polymer film, i.e. the pouch, that is half a millimetre disk and with a thermal conductivity of $0.25 \text{ W K}^{-1} \text{ m}^{-1}$.

The reversible heat sources are considered to be evenly distributed in the two electrodes. The ohmic resistance is considered evenly distributed throughout the electrolyte. Ohmic source terms are neglected elsewhere in the battery model. This is a common assumption in thermal electrochemical models, because as a rule of thumb; an electrode material with good electrochemical-catalytic properties is recognized by its high electronic conductivity. It means that for simplicity, we allocate all ohmic resistance of the battery to the electrolyte. Within the range of operating current we consider the Tafel overpotentials to be equally distributed between the two electrodes.

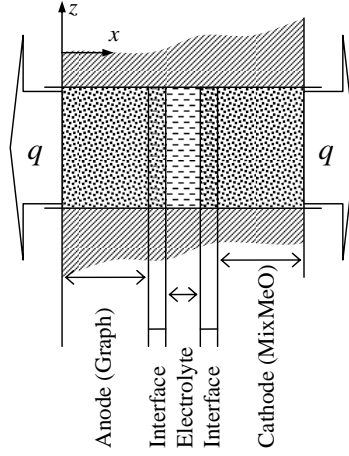


Figure 2: Li-ion model geometry.

The thermal conductivities for the electrode materials are taken from the results obtained in this report. Considering that the electrolyte is very similar to ionic liquids and oils, the thermal conductivity of the electrolyte in the electrolyte region is considered to be in the range of $0.1\text{-}0.5 \text{ W K}^{-1} \text{ m}^{-1}$ and the polymer separator in the order $0.2\text{-}0.3 \text{ W K}^{-1} \text{ m}^{-1}$. For instance; the thermal conductivity of silicon oil, ethylene glycol and polyethylene are 0.1 , 0.25 and $0.5 \text{ W K}^{-1} \text{ m}^{-1}$ [45], respectively, thus making the proposed thermal conductivity (of $0.2 \text{ W K}^{-1} \text{ m}^{-1}$) reasonable.

Modeling Software The modeling was done using COMSOL Multiphysics 4.2a using Fourier heat transfer in solids at stationary state. In practice, this means that Fourier's law, Eq. 7, is solved for each layer and interface of the sketch in Fig. 2.

$$\frac{\partial q}{\partial z} + \dot{P}_{Dissip.} = \frac{\partial}{\partial z} \left(k \frac{\partial T}{\partial z} \right) + \dot{P}_{Dissip.} = 0 \quad (7)$$

where q is the heat out of an infinitely thin layer, k is the thermal conductivity of that layer, T is the temperature, z is thickness direction and $\dot{P}_{Dissip.}$ is the power dissipated as heat in that infinitely thin volume, respectively. Comsol solves this equation inside layers which in turn means that contact resistances are dealt with as extremely thin layers with very low thermal conductivities. Equation 7 is then, again, solved for by a rectangular mesh assuming secondary polynomial functions along the mesh lines. Because of the linear coupling of the heat sources, the uniform distribution within each sub-domain, the insulating boundaries, and the use of quadratic mesh, the model is mesh independent and requires only one element per layer.

Results and Discussion

Thermal Conductivity Measurements

Table 4: Measured thermal conductivity and double contact resistivity of Li-ion secondary battery electrode components at 9.3 bar compaction pressure and ~ 295 K.

Sample Name	Dry		Soaked	
	k_i^{Dry} / $\text{WK}^{-1}\text{m}^{-2}$	$R_{Sample-App}$ / $10^{-4}\text{K m}^2\text{W}^{-1}$	k_i^{Dry} / $\text{WK}^{-1}\text{m}^{-2}$	$R_{Sample-App}$ / $10^{-4}\text{K m}^2\text{W}^{-1}$
LiCoO ₂	0.36±0.03	1.1±0.3	1.10±0.06	0.88±0.07
SLP50	0.30±0.01	0.34±0.17	0.89±0.04	0.43±0.11
CCRAW	0.07±0.01	-	0.36±0.01	-
CC2700	0.41±0.02	-	1.26±0.07	-

Thermal Conductivity The through plane thermal conductivity, k_i , of the LiCoO₂ cathode material at zero charge, the SLP50, the CCRAW and the CC2700 carbon anode materials are given in Table 4 along with the thermal contact resistances towards the apparatus, $R_{Sample-App}$, (for the two commercial materials only). When soaking the electrode materials in the electrolyte solvent not containing any reactive salts, the anode and cathode thermal conductivities were determined to be 1.10 ± 0.06 , 0.89 ± 0.04 , 0.36 ± 0.01 and 1.26 ± 0.07 $\text{W K}^{-1}\text{m}^{-1}$ for LiCoO₂, SLP50, CCRAW and CC2700, respectively. The materials that do not contain any electrolyte solvent have a thermal conductivity of less than a third of those with residual electrolyte solvent. Compared to the few other reported and estimated values found in the literature, in the order $0.9\text{-}32$ $\text{W K}^{-1}\text{m}^{-1}$ [17, 30–32], we report values in the lower end. Because of this mismatch with the literature and that some of the measurements reported in the literature have been questioned [8], our methodology and validation of experiments becomes important. We return to this point later in this section.

Comparing the measured values of the dry materials to those that were soaked in electrolyte solvent, one can see that the electrolyte solvent increases the thermal conductivity by a factor between three and four. Alrahsdan et al. [17] had the electrode material saturated with paraffin, leading to a measured thermal conductivity of $10\text{-}15$ $\text{W K}^{-1}\text{m}^{-1}$. Pouring electrolyte solvent onto the electrode material and next placing a second dry electrode on top, as in the present paper, leads only to a partial saturation of the electrodes. From other studies with porous materials it is known that replacing air filled pores only partly with a liquid (e.g. water), the thermal conductivity of the material increases with a factor between two and four depending on the materials [5, 9, 28, 36]. Electrolyte solvent partly filling the pores leading to an increase in thermal conductivity of a factor between three and four, as is seen in this study, is thus very reasonable. Complete saturation will probably increase the thermal conductivity even further, as seen by Alrahsdan et al. [17]. Moreover, it has been demonstrated that polymers filled with aligned carbon fibres have a thermal conductivity in the range of $0.3\text{-}10$ $\text{W K}^{-1}\text{m}^{-1}$, depending on the volumetric carbon fibre filling fraction [46]. Nevertheless, our choice in wetting the electrode material is very similar to the traditional manner (i.e. assembling in our laboratory inside a glove box) and therefore the thermal conductivity reported here suggests that the thermal conductivity of Li-ion battery electrodes is in the order of 1 $\text{W K}^{-1}\text{m}^{-1}$ or lower.

Another very important effect reported in this study is the effect of heat treating the Carbon Cone material (CCRAW) in Ar at 2700K . For the dry material, the thermal conductivity increased by a factor more than five, while this effect is only 3.5 when introducing

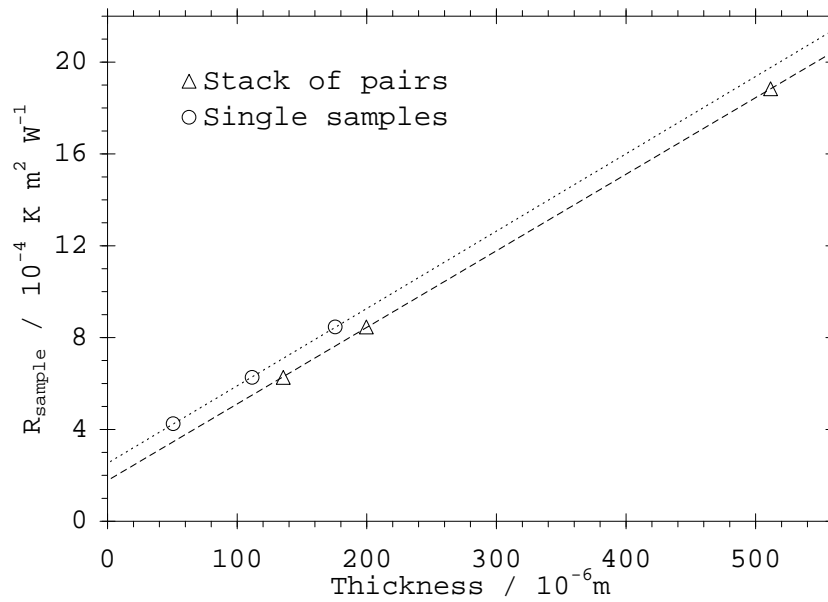


Figure 3: Thermal resistance of single and pairwise stacked SLP50 samples as function of thickness.

electrolyte solvent. The only change is the phase of the carbon in certain regions of the cones/discs. This suggests that attention should also be brought to possibilities with designing and engineering the anode electrode material with respect to thermal conductivity. Possibilities of increasing thermal conductivity is of course a secondary priority compared to the battery capacity, and is also dictated by, the requirements for the battery kinetics. In this instance CC2700 is also in this primary perspective superior to CCRAW.

Measurement validation In the experimental procedure we are interested in the thermal conductivity of the electrode materials. We have chosen to pairwise stack the electrode material films such that they face each other with their Cu or Al film on the outside, sandwiching each paired electrode material. Then we subtract for the thickness of the metal films. The thickness of the metal films had to be subtracted because the thermal resistance of these layers give (almost) no contribution to the thermal resistances. In other words, if not accounting for this thickness contribution we would end up with the wrong gradient of the thermal resistance as a function of thickness. The correctness of this procedure and assumptions are confirmed experimentally in Fig. 3. The single layers and the pairwise stack gives thermal conductivities of 0.297 ± 0.006 and $0.300 \pm 0.003 \text{ WK}^{-1}\text{m}^{-1}$, respectively. The thermal conductivity is the inverse of the gradient of the trend lines in Fig. 3. One can see that whether we changed the thickness of the double layered SLP50 or pairwise stack this anode material, we measure precisely the same thermal resistance as a function of (metal film corrected) thickness. This is an important result of this paper because it validates our chosen pair-wise measurement procedure.

An additional comment to Fig. 3 is that the thickness measurement is calibrated on a daily basis. It is common that the double standard deviation for this type of measurement is 5-10 μm within each series, see e.g. [29]. Beyond this level of uncertainty, the apparatus

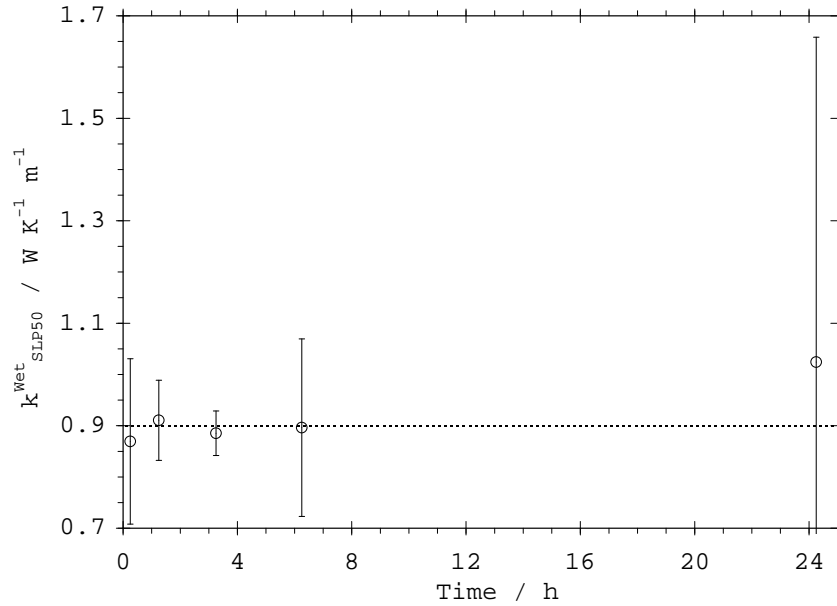


Figure 4: Measured thermal conductivity for SLP soaked in electrolyte solvent.

can fluctuate with up to $15 \mu m$ between two days. The difference between the two lines can be described as a systematic shift in thickness for one of the series, meaning that the calibration one day can have led to a systematic increase in thickness for all the stacked samples, a systematic reduced thickness observation for the varying thickness samples or both. The important part is that the change in thickness within each measurement series is consistent. This is important because it is the slope of the regression rather than the absolute thickness and absolute thermal resistance that is used for retrieving the thermal conductivity. Hence this systematic deviation does not affect the validity of the chosen procedure for thermal conductivity measurements.

Adding electrolyte solvent by dripping it onto the electrode surfaces followed by measuring thermal resistances of wrapped-up stacked pairs of electrodes introduce a new uncertainty. When will the relatively volatile electrolyte solvent evaporate and when will it fully and in a steady manner partially fill the pores? Figure 4 shows measured thermal conductivities obtained a little more (15 min) than 0, 1, 3, 6 and 24 hours after the electrolyte solvent was added to the electrode samples. Each of the thermal conductivity values were obtained from inverse regression lines like the one of Fig. 3 and one can see that the electrolyte solvent wets the electrode SLP50 material very rapidly and that this is stable for several hours, at least with respect to the impact it has on the thermal conductivity. One day after the electrolyte solvent was added to the electrode material, the change in thermal conductivity is scattered and the estimated thermal conductivity is estimated to $1.0 \pm 0.6 W K^{-1} m^{-1}$. The scatter in the value is, according to our understanding, due to depletion of the electrolyte solvents possibly because of vaporisation or drainage. The values measured between one hour and a little more than three hours after the electrolyte solvent was added were by far more reproducible and with little spread compared to those taken immediately after assembly and those taken later than four hours. Already after 6 hours, the measurement indicated loss of electrolyte solvent, both in terms of the reported thermal conductivity and the thermal contact resistance between the stack and the apparatus. This can be seen

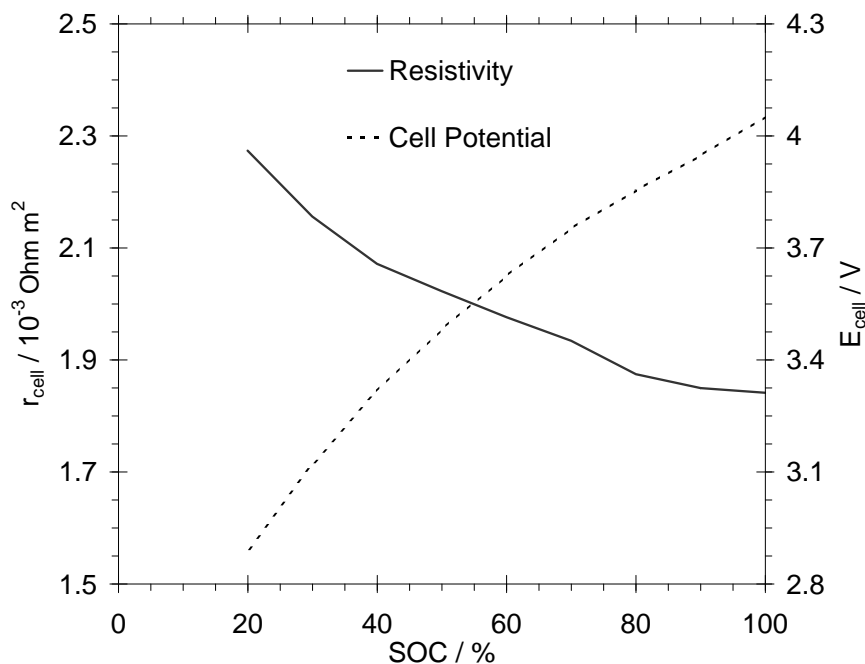


Figure 5: Open circuit potential and cell resistivity of the pouch battery as a function of the state of charge, SOC.

from the plotted thermal conductivities and regression double standard deviations in Fig. 4. Hence, the procedure for the other materials was to measure after 0, 1 and 2 hours after the electrolyte solvent was added.

Dripping electrolyte solvent onto the electrodes in the way that was done in this study could lead to electrolyte solvent being present between the samples and the apparatus, thus significantly lowering the thermal contact resistance between the sample and the apparatus, $R_{\text{Sample-App}}$. From Table 4 one can see that this happened neither in the case of the cathode material (1.1 ± 0.3 vs 0.88 ± 0.07) nor in the case of the SLP50 anode material (0.34 ± 0.17 vs 0.43 ± 0.11), making us confident that in any instance our chosen procedure was theoretically and methodically sound.

The Pouch Cell

Due to manufacturer recommendations, the pouch cell was tested at up to 2C charge and discharge rates.¹ Hence, we were interested in modelling heat aspects of this rate and higher. This section deals with obtaining these necessary values for this modelling.

Thermal, Electrochemical and Thermodynamic Data During the experiments in the present investigation, the state of charge, SOC, range was between 20 and 100 %. The open circuit potential of the battery and the resistivity of the battery was logged and are shown in Fig. 5. It can be seen that the resistivity changes between 1.8 and 2.3 mOhm m^2 and that the

¹1C corresponds to the current required to discharge the battery in one hour.

Table 5: Overview of dimensions relevant for the pouch cell battery model based on measured thickness and thermal conductivities.

Property	CCRAW		SLP50		CC2700		LiCoO ₂		Elec. lyte
	Dry	Wet	Dry	Wet	Dry	Wet	Dry	Wet	
$k / \text{WK}^{-1}\text{m}^{-2}$	0.07	0.36	0.30	0.90	0.41	1.26	0.36	1.10	0.20
$\delta_{layer} / \mu\text{m}^{-1}$	95	95	95	95	95	95	80	80	15
$R_{Th.} / 10^2 \text{m}^2\text{KW}^{-1}$	13.6	2.6	3.2	1.1	2.3	0.8	2.2	0.7	0.8

available open circuit potential was between 2.9 and 4 V, depending on the SOC. In the thermal modelling calculations we used a value of 2 mOhm m².

As is recognised in many studies, the ohmic heat and the reversible heat constitute the main heat sources in a Li-ion battery at high currents [8, 24, 30, 38]. Viswanathan et al. reported a value for the reaction entropy of 9 J K⁻¹ mol⁻¹ for a Li-ion battery mixed nickel manganese cobalt oxide based cathode, also known as NMC. [25] In Appendix B we experimentally confirm this value and thus choose to use this for our thermal analysis.

If considering that a NMC based battery, as the one used in our experimental set-up, has an internal resistance of 2 mOhm m², a reaction entropy with an absolute value of 9 J mol⁻¹ K⁻¹ and a Tafel overpotential of $(-0.0415 + 0.0665\log[j])$ V the stationary heat flux out of the pouch cell outer surface can be calculated using Eqs 8 and 9. In these two equations n refers to the amount of unit cells in the stack. Equation 10 refers to the temperature difference in the air flowing on the pouch cell surface.

$$q_{charge} = \left(-\frac{T\Delta S}{F}j + r_{cell}j^2 + \eta j \right) \frac{n}{2} \quad (8)$$

$$q_{discharge} = \left(\frac{T\Delta S}{F}j + r_{cell}j^2 + \eta j \right) \frac{n}{2} \quad (9)$$

$$q = h\Delta T_o \Leftrightarrow \Delta T_o = \frac{q}{h} \quad (10)$$

Modelling and Numerical Evaluation

Thermal resistances of the cell Thermal conductivity depends both on the manner materials are assembled and the intrinsic thermal conductivity of the material itself. In the first part of this section and from Table 4 one can see that the thermal conductivity of the electrode material is highly dependent on the amount of electrolyte solvent present and also the structure and morphology of the electrode material.

Li-ion cells stacked in a pouch cell can be seen as thermally insulating layers stacked together. They can also be seen as planar heating elements stacked together. Therefore, stacking cells and then next charging (in practice) is equivalent to creating a well insulated heat generating pile. The thickness and the thermal conductivity of the various layers are

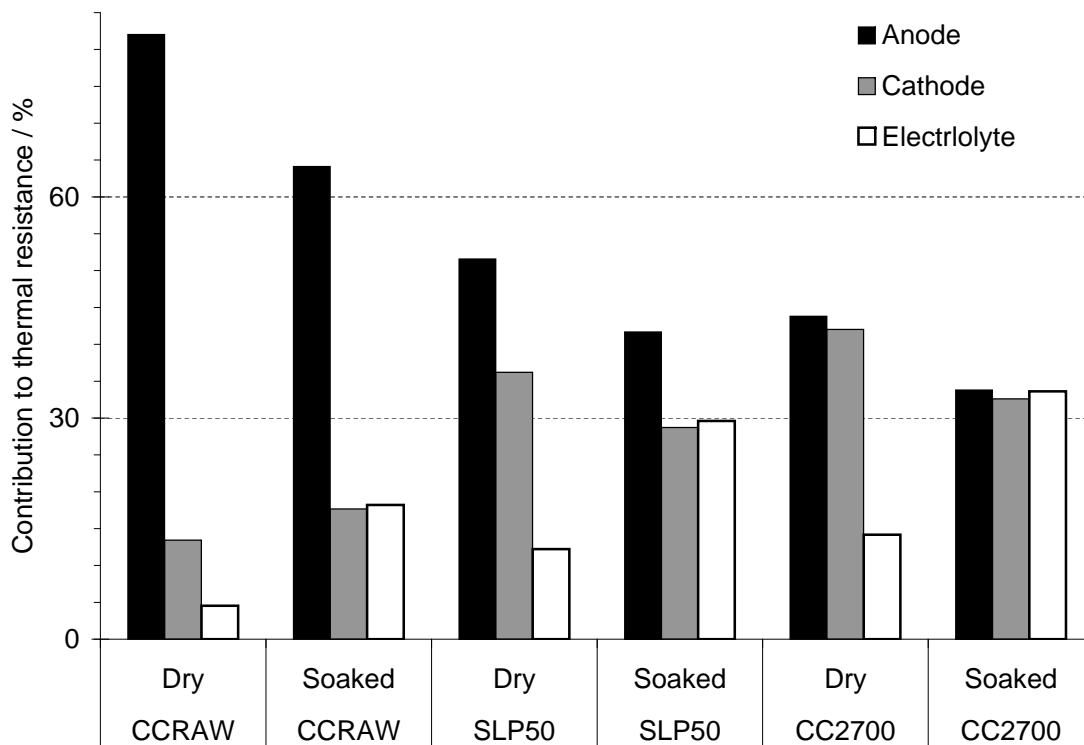


Figure 6: Component relative contribution to the thermal resistance of a possible pouch cell battery. The electrolyte region absolute contribution remains constant in all cases.

important. After all, it is desirable to gain some control over the battery temperature profile. For a given cell at a given load, it is the layers fractional thermal resistance contribution that dictates the temperature profile. The fractional thermal resistance of the electrodes (anode and cathode) and the electrolyte regions in a battery as reported here are given in Fig. 6, both when the electrodes are dry and soaked (wet) with electrolyte solvent. This comparison is of course only a set of estimates, though it is founded on our measurements and common polymer/organic solvent values.

In this study, and as far as electrode thermal conductivity regards, we compare different anode materials and keep the cathode material constant, both for wet and dry materials. In Fig. 6 the various anode materials are compared to the LiCoO_2 material and the electrolyte solvent. When we refer to dry and soaked we indicate whether both electrodes are dry or whether they are saturated with the electrolyte solvent. We consider the electrodes to be saturated with electrolyte solvent when it has been added in our experiments. The thermal conductivity of electrodes that are either completely dry or saturated with electrolyte solvent gives lower and upper boundaries for what the actual thermal conductivities can be, e.g. the thermal conductivity of the cathode material, LiCoO_2 , is between 0.33 and $1.16 \text{ W K}^{-1} \text{ m}^{-1}$. In some instances, when we have investigated commercial Li-ion secondary batteries by opening them, we have observed that the electrode materials appear to be dry. Obviously there must be some electrolyte in the electrode regions in order to supply ionic conduction, but according to our experience the amount is not near the level (saturation) used in our *ex-situ* thermal conductivity measurement experiments. This observation could also be a result of the electrolyte solvent being highly volatile or dollars

Table 6: Current density and total heat flux out of a Li-ion battery with 24 cells

	1C	-2C	2C	4C	8C	10C	12C
$j / \text{A m}^{-2}$	21.1	-42.3	42.3	84.5	169.1	211.4	253.6
$q / \text{W m}^{-2}$	27	125	96	318	992	1466	2177

saved on reducing the electrolyte salt content. However, in some other instances with other cells we have observed droplets of electrolyte (solvents). Because we sometimes observe almost dry electrodes when examining commercial batteries, it may appear reasonable to think that the thermal conductivity of the electrode material is closer to the value measured for the dry samples. However, the thermal conductivity of porous materials is less straight forward and an assumption of proportionality between the amount of liquid and the thermal conductivity is wrong [28]. What is found to be the most important factor for a change in thermal conductivity of porous carbon materials is the contact between the solids [5, 28]. Hence, the results given for each electrode material (dry and soaked) only give the lower and upper boundaries for what the thermal conductivity actually is.

Moreover, as already explained, the thermal resistance of a layer is given by the thickness divided by the thermal conductivity. Hence, it is obvious that not only the thermal conductivity is important but also the thickness of each of the layers. This is illustrated in Fig. 6. The advantage of considering thermal resistances in addition to thermal conductivities and layer thickness is that the resistances are additive in series. We assume the thermal conductivity of the electrolyte-separator region to be rather low, but since this layer is also very thin the overall impact is reduced. In order for the electrolyte region to become important to the overall thermal resistance, we need to combine it with soaked LiCoO₂ and soaked CC2700 electrode materials. Comparing the case with dry CCRAW to that of soaked CC2700 the anode material is developed from constituting more than eighty percent of the total thermal resistance to being equal to the other two layers of the unit cell. The electrolyte solvent is estimated to have a thermal conductivity of $0.2 \text{ W K}^{-1}\text{m}^{-2}$. In light of the range of thermal conductivities for most organic liquids this is an intermediate value and the electrolyte region also typically contains a polymer mesh to separate the electrodes. Also, for a polymer, a thermal conductivity of $0.2 \text{ W K}^{-1}\text{m}^{-2}$ is a reasonable typical value and this parameter is also to a very limited degree a subject to thermal conductivity enhancement. Thus, because of the large impact on the cell thermal resistance and the possibilities within thermal conductivity modification by engineering, the thermal conductivity of the electrodes is the most interesting thermal property of the Li-ion secondary battery. That is, off course, if we ignore phase changing additives inserted for heat adsorption during charging and high loads [17].

It may seem that one approach to lower the thermal resistance is lowering the electrode material thickness further. However, these materials also act as energy storage volumes. Therefore, manufacturing electrodes such that they contain a lot of electrolyte is, in the light of the present results, the most simplistic route to increase the overall thermal conductivity of Li-ion secondary batteries.

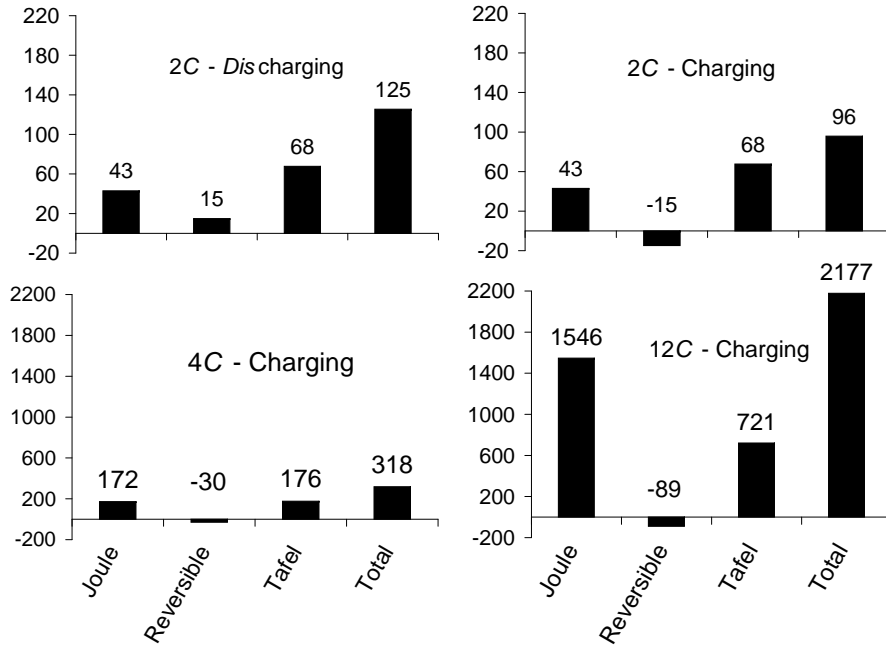


Figure 7: Heat generated during charging and discharging of two Li-ion secondary batteries. Note the difference on the axis values for the upper and the lower diagrams: At $\pm 2C$ the total heat release is close to the heat accumulation is the same, but when the charging of 12C the heat release is overwhelming.

Heat Sources and Sinks in a Li-ion secondary battery A Li-ion battery is subject to internal heating or cooling when charged or discharged depending on the current and the properties of the battery. This is illustrated in Fig. 7. The two upper charts consider heat contribution from discharging and charging at a current density of $\pm 42.4 \text{ A m}^{-2}$ ($\pm 2C$) while the two lower charts consider charging at current densities of 86 and 254 A m^{-2} (4 and 12C). Note that the secondary axes are different for the upper and the lower pair of graphs and that they differ by one order of magnitude. The current equivalent to 12C may appear a little exaggerated. However Sabbah et al. have reported a study where a current density equivalent to 6.7C was applied [47] and the 12C value corresponds to a complete charging cycle time of five minutes, which is by many considered a target for Battery Electric Vehicles, BEV [1].

The ohmic heating term is proportional to the squared current, j^2 . Since the reversible heat and the Tafel heat, to a first order approximation, are linear functions of the current, the ohmic heat term is dominating at higher current densities. Looking at Figure 7, the ohmic heat constitutes fifty percent of the overall energy dissipation already at a current equivalent to 4C. At 12C this term constitutes around 75% of the total heat generation of the NMC battery in this study. If a battery using $\text{Li}_x\text{Co}_{1-x}\text{O}$ anode, the reversible heat term could be expected to be four times larger than for a NMC battery. If so, this would lower the total heat generation by $\sim 14\%$ representing a cooling effect in the battery during charging at 12C. Although a cooling fraction of $\sim 14\%$ is not immense, it is still worth considering – batteries age faster at higher temperature and any cooling contribution should be embraced.

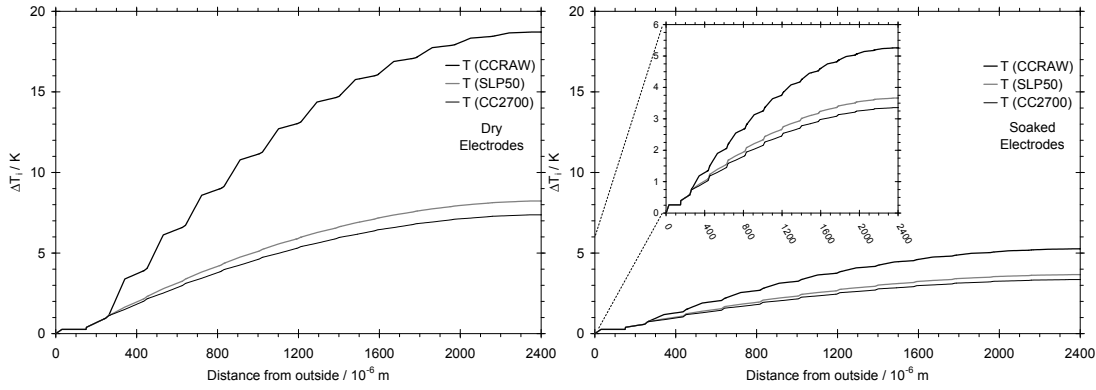


Figure 8: Temperature profiles of single cell Li-ion batteries when cooled at both sides (left) during charging at 12 C current. To the left in the figure we consider thermal conductivities of dry electrode materials and to the right we consider thermal conductivities of the materials soaked in electrolyte solvent. Superimposed in the right graph is an zoomed view of the same graph.

Internal Temperature Profiles When heat is generated inside a volume, internal temperature gradients will necessarily emerge. Deploying the given Fourier model along with the measured thermal conductivities we can get some insight to these temperature profiles.

Figure 8 shows internal temperature profiles modeled with the geometries and heat sources of the commercial Li-ion pouch cell for different measured thermal conductivities. The model considers charging at 12C. To the left in the figure we consider thermal conductivities of dry electrode materials and to the right we consider thermal conductivities of the materials soaked in electrolyte solvent. Superimposed in the right figure is an enlarged version of the same graph. Hence one can compare the difference between soaked and dry materials and at the same time study the modeled temperature regimes.

Because the heat sources are, more or less, evenly distributed in the insulating layers, the internal temperature profile will always be non-linear and far steeper across the outer cells than the inner cells. Correspondingly, at the middle of the battery, the temperature is isothermal. In Fig. 8 we show only half the temperature profiles because it is symmetrical around the battery centre cell. At first sight, Fig. 8 predicts internal temperature differences between 2.5 and 19 °C. However, the scenario of the temperature profile with dry CCRAW electrode material is not likely because the annealing is required for the material electric and electrochemical properties anyway, i.e. the raw material will never be used in a battery anode in the first place. It is shown here in order to illustrate the impact of engineering the thermal conductivity of one of the battery component materials. What is likely, however, is an internal temperature difference of 3-8 °C. Considering cooling the battery with air, an ambient temperature difference in the air of around 30-35 °C is likely with at the best heat transfer coefficients [8], thus suggesting that a total temperature difference between the air and the battery core of up to 40-45 °C is not unlikely if charging at 12C. Temperature differences in this range is of course the extreme scenario. Hence the battery temperature is manageable. One does, however, expose the battery to temperatures that can lead to reduced life time or increased degradation and care should be sought.

Relevance for Thermal Runaway and Degradation With the most extreme temperature gradients suggested here, a thermal runaway appears unlikely at first. However, some thermal runaway mechanisms have similarities to effects of increased temperature and at high charging rates. It is therefore useful to review some of these mechanisms here.

According to Tobishima, a thermal runaway occurs when reactions inside a battery dissipates more heat than the components can transfer and the materials of the battery starts to decompose in an uncontrolled manner. [48], e.g. evaporation of electrolyte solvents. The first part of this definition describes any initial non-stationary thermal model. With constant heat dissipation, the system will reach an equilibrium between the total temperature difference, the heat flux and the thermal resistance of the components (between the heat source and a heat sink). This is analogous to the examples given in Section . It is when this equilibrium allows for a maximum temperature so high that additional exothermic reactions are initiated, and the heat production becomes out of control, that we have a thermal runaway.

For instance, if the electrode separator should melt (which occurs at 125° for polyethylene) the cell is very likely to short circuit. This could potentially initiate a thermal runaway [48]. Moreover, at temperatures close to the melting point the separator could for instance weaken and deform to an extent where short circuiting is a result. In order to prevent scenarios like this, most modern Li-ion secondary batteries deploy a separator that will irreversibly seal a small area of the electrolyte at much lower temperatures, thus acting as a local fuse. This scenario must be avoided as the battery will be irreversibly damaged, first locally and later entirely due to the corresponding uneven current densities. Imagine uneven cooling, in the first place, allowing locally increased temperature, drying of the electrodes, increased local thermal conductivity, and destruction by this fuse mechanism. A corresponding increase in the local current density of e.g. 10% will lead to an increase of the ohmic heat of 21%.

Another possible scenario, that is interesting in the light of the results of this paper, is displacement of electrolyte within the battery. In some cases, for instance, we have observed that commercial battery electrode materials are not always completely soaked in electrolyte. We know that the electrolyte solvent is volatile and have seen that evaporation disturbs our experiments and, on top of this, we have just learnt that the amount present in the electrode material is very important for the thermal conductivity. Thus, a scenario where electrolyte in time becomes depleted in the inner layers and enriched in the outer layers of a prismatic, or rolled up for that matter, battery can occur. This, in combination with locally disturbed external air cooling, would result in the battery electrolyte separator fuse to go off and subsequently destroy the battery.

There are many more scenarios that lead to thermal runaway [48], but to our knowledge none of them considers the impact of thermal conductivity of the electrode materials. The chosen model scenario in this report might be seen as a little extreme, using high charging current and low reversible heat adsorption, however not unlikely. (Besides, we have already seen that the reaction entropy of the battery is actually not that important (14 %) at these extremely high charging currents.) The aim of this paper is to discuss the importance of thermal conductivity of electrode materials and the possibility to engineer such. Even if high rate charging takes place only a short part of the life time of a battery, the thermal gradients imposed can be lowered with the right electrode materials and thus some thermal

runaway scenarios be avoided.

Conclusion

The thermal conductivity of Li-ion battery electrodes were measured both for dry samples and for materials containing electrolyte. The thermal conductivity was found to vary between 0.07 and 1.10 W K⁻¹ m⁻¹. Heat treatment at 3000K was found to increase the thermal conductivity by a factor of almost five for one of the carbon anode materials (CCRAW/CC2700). Adding electrolyte solvent to the electrode materials, the thermal conductivity increased by a factor of almost three. The thermal conductivity of secondary Li-ion batteries is likely to vary within the range of 0.5-1.1 W K⁻¹ m⁻¹ throughout the lifetime. It is important to know that this property can be engineered and controlled.

A thermal model in combination with laboratory experiments suggested that temperature differences larger than 40 K between the battery centre and the ambient air is likely when charging a battery completely in five minutes (equivalent to 12C). Comparing the potential for improving the cooling of air cooled pouch cells, we consider the temperature gradients outside the battery the most challenging, though both externally and internally are important to assess. This paper presents information that is essential for the latter.

Acknowledgement

The Norwegian Research Council is acknowledged for financial support, FRIENERGI, grant number 197598, and RENERGI, grant number 164466/S30.

The authors thank TIMCAL Graphite & Carbon and n-Tec for providing the carbon materials in this study. We also acknowledge Arkema and Circuit Foil for providing us with the electrode binder material and copper current collector, respectively. Finally, we would (once more) show our gratitude towards the research council of Norway for partially financial support through the industrial-PhD program.

References

- [1] F.T. Wagner, B. Lakshman, and M.F. Mathias. *J. Phys. Chem. Lett.*, 1:2204–2219, 2010.
- [2] C.E. Thomas. *Int. J. Hydrogen Energy*, 34:6005–6020, 2009.
- [3] S. Aktas, D. J. Fray, O. Burheim, J. Fenstad, and E. Açma. *Mineral Processing and Extractive Metallurgy (Trans. Inst. Min. Metall. C)*, 115:95–100, 2006.
- [4] C.J. Bapat and S.T. Thynell. *ASME, J. Heat Transfer*, 129:1109–1118, 2007.
- [5] O. Burheim, G. Elila, J.D. J. D. Fairweather, A. Labouriau, S. Kjelstrup, and J.G. Pharoah. *J. Power Sources*, 221:356–365, 2013.
- [6] G. Zhang and S. G. Khandlikar. *Int. J. Hydrogen Energy*, 37:2412–2429, 2012.

- [7] W. Fang, O.J. Kwon, and C.-Y. Wang. *Int. J. Energy Research*, 34:107–115, 2010.
- [8] T.M. Bandhauer, S. Garimella, and T.F. Fuller. *J. Electroch. Soc.*, 158:R1–R25, 2011.
- [9] Odne S. Burheim, Mesut Aslan, Jennifer S. Atchison, and Volker Presser. *J. Power Sources*, 246:160–166, 2014.
- [10] T. Doi, B. Zhou, L. Zhao, S. Okada, and J. Yamaki. *Electroch. Communications*, 11:1405–1408, 2009.
- [11] Y.H. and Song J.H. Kim, K.J. Kim, Y.N. Jo, J.-S. Kim, and Y.-J. Kim. *J. Power Sources*, 195:6075–6080, 2010.
- [12] D. Belov and D.-T. Shieh. *J Solid State Electrochem.*, April:DOI 10.1007/s10008–011–1391–y, 2011.
- [13] Y.-H. Cho, K. Kim, S. Ahn, and H.K. Liu. *J. Power Sources*, 196:1483–1487, 2011.
- [14] K.J. Kim, J.-H Kim, M.-S. Park, H.K. Kwon, H. Kim, and Y.-J. Kim. *J. Power Sources*, 198:298–302, 2012.
- [15] I. Krupa, G. Mikova, and A.S. Luyt. *European Polymer J.*, 43:4695–4705, 2007.
- [16] R. Kandasamy, X.Q. Wang, and A.S. Mujumdar. *Appl. Thermal Engin.*, 27:2822–2832, 2007.
- [17] A. Alrashdan, A.T. Mayyas, and S. Al-Hallaj. *J. Mat. Processing Technol.*, 210:174–179, 2010.
- [18] J. Van Mierlo, G. Maggetto, and Ph. Lataire. *Energy Conversion and Management*, 47:2748–2760, 2006.
- [19] Møller-Holst S. Svensson, A.M., R. Gløckner, and O. Maurstad. *Energy*, 32:437–445, 2007.
- [20] S. Campanari, G. Manzolini, and F.G. de la Iglesia. *J. Power Sources*, 186:464–477, 2009.
- [21] S. Kjelstrup and A. Røsgjorde. *J. Physical Review: Part B*, 109:9020, 2005.
- [22] O. Burheim, P.J.S. Vie, S. Møller-Holst, J.G. Pharoah, and S. Kjelstrup. *Electrochimica Acta*, 5:935–942, 2010.
- [23] O. Burheim, S. Kjelstrup, J.G. Pharoah, P.J.S. Vie, and S. Møller-Holst. *Electrochimica Acta*, 5:935–942, 2011.
- [24] N. Sato. *J. Power Sources*, 99:70–77, 2001.
- [25] V.V. Viswanathan, D. Choi, D. Wang, W. Xu, S. Towne, R.E. Williford, J.-G. Zhang, J. Liu, and Z. Yang. *J. Power Sources*, 195:3720–3729, 2010.
- [26] K. Kinoshita. Intersci., New York, 1992.
- [27] Y. Chen and J. W. Evans. *Electrochimica Acta*, 39:517–526, 1994.
- [28] O. Burheim, H. Lampert, J.G. Pharoah, P.J.S. Vie, and S. Kjelstrup. *ASME J. Fuel Cell Sci. & Technol.*, 8:021013–1–11, April 2011.

- [29] O.S. Burheim, H. Su, S. Pasupathi, J.G. Pharoah, and B.G. Pollet. *Int. J. Hydrogen Energy*, 38:8437–8447, 2013.
- [30] S.-C. Chen and C.-C. Wan. *J. Electroch. Soc.*, 153:A637–A648, 2006.
- [31] R. Mahamud and C. Park. *J. Power Sources*, 196:5685–5696, 2011.
- [32] H. Maleki, S.A. Hallaj, J.R. Selman, R.B. Dinwiddie, and H. Wang. *J. Electroch. Soc.*, 146:947–954, 1999.
- [33] Sun Ung Kim. *PhD Thesis - Univ. of Michigan*, Ch 4:50–87, 2013.
- [34] N. Zamel, E. Litovsky, S. Shakhshir, X. Li, and J. Kleiman. *Int. J. Hydrogen Energy*, 36:12618–12625, 2011.
- [35] M. Khandelwal and M.M. Mench. *J. Power Sources*, 161:1106–1115, 2006.
- [36] O. Burheim, P.J.S. Vie, J.G. Pharoah, and S. Kjelstrup. *J. Power Sources*, 195:249–256, 2010.
- [37] S.C. Nagpure, R. Dinwiddie, S.S. Babu, G. Rizzoni, B. Bhushan, and T. Frech. *J. Power Sources*, 195:872–876, 2010.
- [38] X. Zhang. *Electrochimica Acta*, 56:1246–1255, 2011.
- [39] P. Teertstra, G. Karimi, and X. Li. *Electrochimica Acta*, 56(3):1670–1675, 2011.
- [40] J. Ramousse, O. Lottin, S. Didierjean, and D. Maillet. *Int. J. of Thermal Sci.*, 47:1–6, 2008.
- [41] R. B. Bird, W. E. Stewart, and E. N. Lightfoot. Jon Wiley & Sons, Inc., 2nd edition, 2006.
- [42] T. Garberg, S. N. Naess, G. Helgesen, K. D. Knudsen, G. Kopstad, and A. Elgsaeter. *Carbon*, 46:1535–1543, 2008.
- [43] Engineering Toolbox Website. www.engineeringtoolbox.com/thermal-conductivity-d_429.html, February 28, 2012.
- [44] D. Bansal, F. Cassel, F. Croce, M. Hendrickson, E. Plichta, and M. Salomon. *J. Phys. Chem. B*, 109:4492–4496, 2005.
- [45] R.C. Weast. CRC PRESS, Inc., 58th edition, 1977.
- [46] F. Robinson, J. G. Cevallos, A. Bar-Cohen, and H. Bruck. *Proceedings of the ASME 2011 Int. Mechanical Engineering Congress & Exposition IMECE2011*, IMECE2011-65684:1–10, 2011.
- [47] R. Sabbah, R Kizilel, J. R. Selman, and S. Al-Hallaj. *J. Power Sources*, 182:630–638, 2008.
- [48] S. Tobishima. *Secondary Batteries – Rechargeable Systems – Lithium-Ion*, pages 409–417, 2009.
- [49] P. Atkins and J. Paula. Oxford University Press, 7th edition, 2002.
- [50] K.S. Fjørland and S. Fjørland, T. Kjelstrup. Tapir Academic Press, Trondheim: Reprint from Jon Wiley and Sons, Inc., 2001.

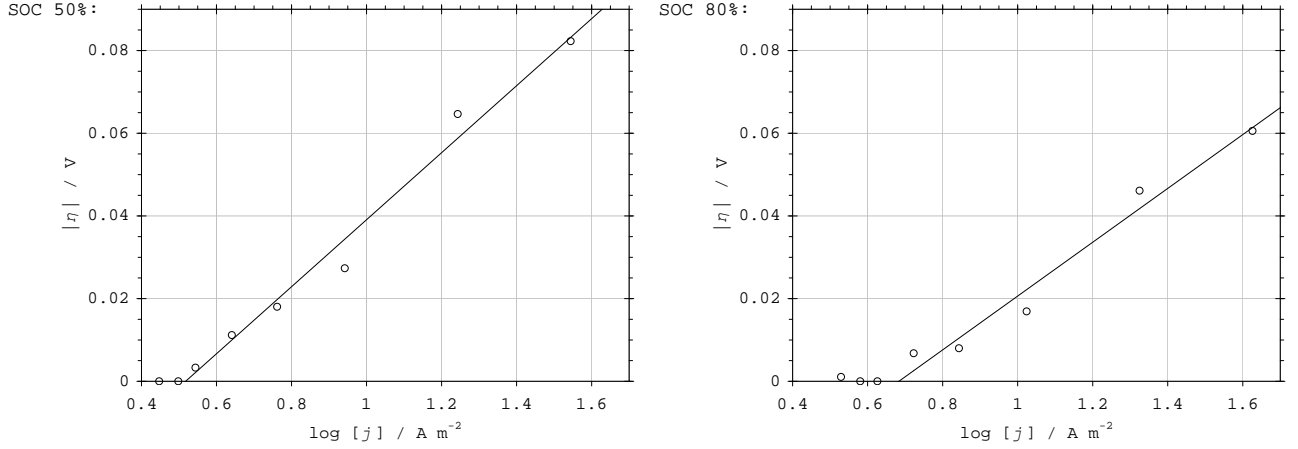


Figure 9: Measured overpotential and corresponding Tafel regression lines.

Table 7: Tafel equation coefficients by Eq. 11 obtained at different state of charge, SOC.

SOC	a / V	b / V decade ⁻¹
50%	-0.039±0.010	0.068±0.009
80%	-0.044±0.015	0.065±0.013

A Determination of Tafel Overpotential

The Tafel overpotential equation, Eq. 11, can be derived from the Butler-Volmer equation when the current density is significantly larger than the equilibrium current density, also known as the exchange current density, j_0 . The theory for the Tafel and Butler-Volmer overpotential [49] is only valid for a single electrode reaction and only when the electron transfer is determining the reaction rate (j). Here, however, we deploy it on the battery total overpotential. We can do this under the assumption that one of the electrodes has an overpotential that is by far larger than the overpotential of the other electrode, i.e the rate determining step of the battery is electron transfer in one of the electrodes. Which of the electrodes and electrode reactions that determines the Tafel behaviour is not necessary for the results in this paper. It is therefore not taken into further considerations.

$$\eta = a + b \log [j] \quad (11)$$

The Tafel coefficients are given for two different state of charge, SOC, in Table 7. One can see that the slope of the Tafel equation (b in Eq. 11) is the same at SOC of 50 and 80%. Within the regression coefficient double standard deviations, one can also see that the constant (a in Eq. 11) remains unaffected by the SOC. However, based on the experiments undertaken for this paper there is no significant difference in the Tafel behaviour as a function of SOC within the SOC range of 20 to 100 %.

B Reaction Entropy, ΔS

For any chemical reaction at constant pressure and at a given temperature, the available work is dictated by Gibbs free energy of formation, ΔG . Expressed in terms of total change in energy (reaction enthalpy), ΔH , reaction entropy, ΔS , and temperature, T , the Gibbs free energy of formation is given as;

$$\Delta G = \Delta H - T\Delta S \quad (12)$$

From the Nernst equation ($-nFE = -\Delta G$) we have;

$$E_{cell} = \frac{\Delta H}{F} - T\alpha \quad (13)$$

where F is the Faraday constant and α is the Seebeck coefficient of the battery;

$$\alpha = -\frac{\Delta S}{F} = -\frac{1}{F} \frac{\partial \Delta G}{\partial T} = \frac{\partial E^{OCV}}{\partial T} \quad (14)$$

Hence, from the regression line in Fig. 10 we obtain, as a first order approximation², the reaction entropy equal to $10.4 \pm 0.4 \text{ J mol}^{-1} \text{ K}^{-1}$. Viswanathan et al. reported a reaction entropy of approximately 9 J / K mol [25]. In the presented reaction entropy verification experiment, the measured potential at the higher temperatures underestimates the temperature (due to internal temperature gradients). The lower values are closer to battery isothermal conditions and therefore it is a reasonable assumption that the higher cell voltage values should in reality be shifted to the right - leading to a slightly lower absolute Seebeck coefficient and, correspondingly lower reaction entropy value. [50] Hence, the value for the reaction entropy deployed in the calculations is experimentally verified for the present battery.

²This approximation assumes the reaction enthalpy and the reaction entropy to be independent of temperature, which is equivalent to neglecting the heat capacity of the active electrode material, C_p .

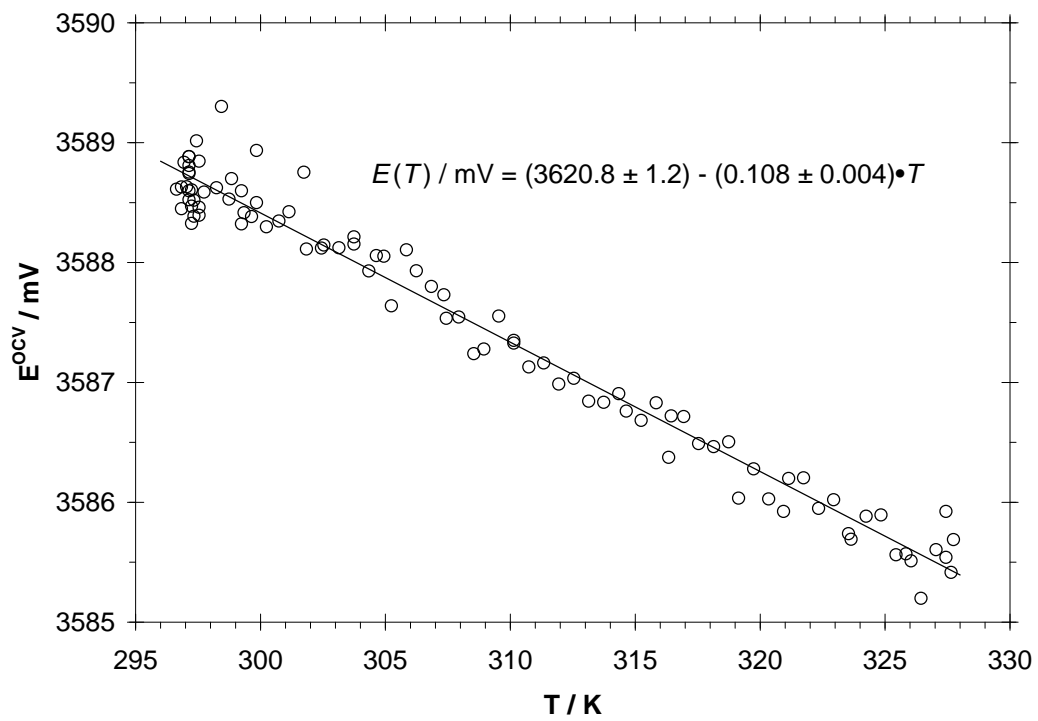


Figure 10: Open circuit cell potential as a function of temperature.